

Optimal design of experiments for a lithium-ion cell: parameters identification of a single particle model with electrolyte dynamics

Andrea Pozzi,^{*,†} Gabriele Ciaramella,[‡]

Stefan Volkwein,[‡] and Davide M. Raimondo[†]

[†]*Dipartimento di Ingegneria Industriale e dell'Informazione,
University of Pavia, 27100 Pavia, Italy*

[‡]*Department of Mathematics and Statistics, University of Konstanz, Germany*

E-mail: andrea.pozzi03@unipv.it

Abstract

Advanced battery management systems rely on mathematical models to guarantee optimal functioning of Lithium-ion batteries. The Pseudo-Two Dimensional (P2D) model is a very detailed electrochemical model suitable for simulations. On the other side, its complexity prevents its usage in control and state estimation. Therefore, it is more appropriate the use of simplified electrochemical models such as the Single Particle Model with electrolyte dynamics (SPMe), which exhibits good adherence to real data when suitably calibrated. This work focuses on a Fisher-based optimal experimental design for identifying the SPM parameters. The proposed approach relies on a nonlinear optimization to minimize the covariance parameters matrix. At first, the parameters are estimated by considering the SPM as the real plant. Subsequently, a more realistic scenario is considered where the P2D model is used

to reproduce a real battery behavior. Results show the effectiveness of the optimal experimental design when compared to standard strategies.

1 Introduction

Battery Management Systems (BMSs) are necessary in order to provide safe and profitable operations in lithium-ion batteries.¹ Advanced BMSs rely on mathematical models whose accuracy is fundamental to achieve high performance. Several models have been proposed in literature to describe the behavior of lithium-ion cells. These can be classified in two main categories: Equivalent Circuit Models (ECMs) and Electrochemical Models (EMs). While ECMs are simple and intuitive, EMs, which describe the chemical phenomena occurring inside a cell, can be far more accurate. The Pseudo Two Dimensional (P2D) model, also known as Doyle-Fuller-Newman (DFN), is a very detailed EM suitable for simulating the behavior of Lithium-ion cells.^{2,3} Different numerical implementations of the P2D have been proposed over the years (e.g. DUALFOIL , LIONSIMBA⁴). The use of simulators to assess the performance of novel strategies is a common procedure in literature.⁵ However, in order to obtain reliable representations of a real process, realistic parameters are required. To this purpose, within the context of Li-ion batteries, Ecker et al.⁶ performed invasive measurements on a commercial cell. In particular, they obtained a complete parameterization of the DFN model by opening the cell under argon atmosphere. While this approach is suitable for building a realistic simulator, it can not be applied in the context of battery control since it could compromise the proper functioning of the cells. On the other side, experiments performed under normal operating conditions, based on voltage measurements only, demonstrated that not all the parameters of the P2D model are identifiable. The structural identifiability and ill-conditioning sources of the DFN model have been analyzed by many authors (see e.g. Bizeray,⁷ where Table 1.1. reports a summary of the literature on the parameter estimation of electrochemical lithium-ion

battery models). In Lopez et al.⁸ for example, the authors rely on the Fisher Information Matrix,⁹ which gives a measure of how much a certain input signal is informative in terms of parameter sensitivity. The authors show that multiple discharging experiments with several currents may improve parameters identification, reducing their variances. However, some parameters of the DFN still remain unidentifiable. Similar results have been obtained by Forman et al.,¹⁰ where the Fisher Information has been used in order to evaluate the accuracy of the DFN parameters estimated using a genetic algorithm. In Zhang et al.¹¹ a sensitivity analysis of up to 30 parameters of the P2D model is conducted and a step-wise experiment is proposed. In particular, the parameters with similar identifiability conditions are estimated in the same step, while assuming the others to be known. The proposed approach exploits genetic algorithm for parameters estimation and provides significant results, although it is validated on synthetic data in absence of measurement error. Note that, even in this favorable scenario it was not possible to identify all the parameters. These results, together with the lack of observability of the P2D model¹², motivate the use of simpler models for control purposes. In Lu et al.¹³ an overview of different simple battery models and parameter identification techniques is presented, while in He et al.¹⁴ and Tian et al.¹⁵ the parameter identification process for an ECM is described. In Torchio et al.,¹⁶ a step response model, suitable for control purposes, is identified using the least squares method. The same authors propose a piece-wise affine approximations of the P2D model.¹⁷ Despite to their simplicity, the use of ECMs and input-output models does not allow to take into account physico-chemical phenomena occurring inside the battery. For this reason, the Single Particle Model¹⁸ (SPM), a simplified electrochemical model, has been considered by many authors. In particular, the observability of the SPM has been addressed by Di Domenico et al.¹⁹ In this work the authors claim that the Lithium concentration states of the SPM with two electrodes are weakly observable from the differential voltage measurement alone. On the other side, the parameters identifiability of the SPM has been discussed by e.g. Bizeray et al.²⁰ In this work, the output voltage has

been linearized around an equilibrium and the parameters grouped into hyper-parameters that can be experimentally identified. A different simplified electrochemical model has been considered in Schmidt et al.,²¹ where a Fisher Information approach in combination with a sensitivity analysis has been used to estimate the identifiability of the parameters.

In this work we rely on the SPM with electrolyte dynamics (SPMe), motivated by the fact that reduced electrochemical models preserve a physico-chemical meaning and provide a good fit. In particular, the authors in Moura et al.²² demonstrated the suitability of SPMe for control and estimation purposes. Nevertheless, model reduction usually comes with a loss of accuracy, which has to be balanced with a proper parameter identification procedure.

In order to obtain high parameters accuracy, a sufficiently exciting input is usually required. The Design of Experiment (DoE) consists in finding the optimal input sequence able to minimize the uncertainty of model parameters.²³ In Liu et al.²⁴ the importance of DoE in the context of control of lithium-ion batteries has been underlined. This topic has been discussed by many authors. In Mendoza et al.²⁵ the thermal cycle of a cell is optimized in order to estimate the entropy coefficient while reducing experimental time and maximizing the Fisher Information. This method has been applied by the same authors in order to identify the parameters of an ECM coupled with a thermal model,²⁶ while the authors in Hametner et al.²⁷ propose an optimal design of experiment for a fuzzy model of a Li-ion cell. The DoE has also been considered by Mathieu et al.²⁸ in order to optimally calibrate the parameters of a battery ageing model. In Park et al.²⁹ the optimal DoE for the complete parametrization of the DFN model is addressed. The parameters are firstly divided into two different sets, accordingly to their characteristic, and an optimal input profile is iteratively selected from an input library in order to maximize the corresponding Fisher Information Matrix. The proposed approach is then experimentally validated. Even in this case, some parameters have not been identified with high accuracy and exhibit a wide confidence interval, thus confirming the need of a simpler model for control purposes.

In this work we propose an optimal DoE for the parameters identification of the SPMe, for which the parameters accuracy remains fundamental in order to achieve high performance in the context of control and state estimation. In the following, we rely on a Fisher Information-based approach. Considering that the generalized inverse of the Fisher Information Matrix provides an approximation of the covariance parameter matrix, we pose a nonlinear optimization problem aiming to minimize the trace of this latter, similarly to what proposed by Korkel et al.³⁰ Differently from Park et al.²⁹ we fully design the input for each time instant, without relying on an a priori library. At first, we consider the SPMe as the real plant, with the output affected by zero mean Gaussian noise. In particular, the accuracy of the estimation is evaluated in terms of mean and variance of the parameters. Within this context, the simulations show the effectiveness of the proposed approach when compared to standard constant current profiles. Results show that the proposed approach can provide a significant improvement in terms of variance reduction and convergence to the true values of the parameters in minimum experimental time. Subsequently, we consider a more realistic scenario, in which a real battery simulator based on the P2D model is assumed to be the real process, while the SPMe is used as model for control and estimation. Within this context, the SPMe parameters needs to be estimated with high accuracy on data collected from the P2D model. Note that the use of a very detailed model (P2D), together with a numerically stable simulation framework (in this paper LIONSIMBA) and a set of realistic parameters, provides important insights on the real battery behavior and allows to estimate whether an approach (e.g. Design of Experiments) will be worth in practice or not (saving a lot of time during the experimental phase). The results highlight that the SPMe, simulated using the parameters from the optimal DoE, presents the best fitting in terms of prediction of the P2D output voltage. Summarizing, the main contributions of this work are the following.

- The use of the optimal DoE approach in order to minimize the covariance of the SPMe estimated parameters and improve the model accuracy.

- We propose a sub-optimal approach so to reduce the computational burden of the nonlinear constrained optimization, which may limit the design of long experiments.

The paper is organized as follows. In Sec. 2 the P2D model is described in detail, while the main equations of the SPMe are recalled in Sec. 3. In Sec. 4 the optimization method based on the Fisher information is presented and in Sec. 5 the benefits of the proposed method are highlighted in simulation, when the SPMe is affected by Gaussian zero mean noise. In Sec. 6 the optimal design of experiment is applied considering the P2D model as the real plant. In Sec. 7 the obtained results are resumed.

2 Pseudo two dimension model

In this section, the main equations used to describe the electrochemical behavior of a Lithium-ion cell are presented. In particular we rely on the well known isothermal P2D model, which is described by a set of nonlinear and tightly coupled Partial Differential and Algebraic Equations (PDAEs).³

A Lithium-ion cell is composed by a superposition of different layers: the cathode (p), the separator (s), and the anode (n). The electrodes and the separator are immersed in an electrolytic solution, thus enabling ionic conduction. In the following, the index $i \in \{p, s, n\}$ is used to refer to the different sections of the battery, whose thicknesses are denoted by L_i . The diffusion process within the solid phase of each electrode is described by Fick's law

$$\frac{\partial c_{s,i}(x, r, t)}{\partial t} = \frac{1}{r^2} \frac{\partial}{\partial r} \left[D_{s,i} r^2 \frac{\partial c_{s,i}(x, r, t)}{\partial r} \right], \quad (1)$$

where $t \in \mathbb{R}^+$ represents the time, $x \in \mathbb{R}$ is the one-dimensional spatial variable along which ions flow, $r \in \mathbb{R}^+$ is the radial direction along which the ions intercalate within the active particles (i.e. the pseudo-second dimension of the model), $c_{s,i}(x, r, t)$ is the lithium

concentration in the solid phase, $D_{s,i}$ is the solid diffusion coefficient. The electrolyte diffusion of ions is given by the following equation

$$\epsilon_i \frac{\partial}{\partial t} c_{e,i}(x,t) = \frac{\partial}{\partial x} \left[D_{\text{eff},i} \frac{\partial c_{e,i}(x,t)}{\partial x} \right] + a_i(1 - t_+) j_i(x,t), \quad (2)$$

where $c_{e,i}(x,t)$ is the electrolytic ion concentration and $j_i(x,t)$ is the ionic flux. Moreover, t_+ defines the transference number and a_i is the specific active surface area defined as

$$a_i = \frac{3(1 - \epsilon_{f,i} - \epsilon_i)}{R_{p,i}}, \quad (3)$$

where $\epsilon_{f,i}$ is the filler fraction, ϵ_i is the electrolyte porosity, $R_{p,i}$ is the particle radius, while $D_{\text{eff},i}$ accounts for the effective diffusion coefficients in the electrolyte. In particular, this latter according to Bruggeman's theory is given by

$$D_{\text{eff},i} = \epsilon_i^p D_e, \quad (4)$$

where D_e is the electrolyte diffusion coefficient, assumed to be constant in c_e , and p is the Bruggeman coefficient. The ionic flux is modeled by a Butler-Volmer equation

$$j_i(x,t) = \begin{cases} 2i_{0,i} \sinh \left[\frac{0.5F}{RT} \eta_i(x,t) \right], & i \in \{p, n\} \\ 0, & i \in \{s\} \end{cases} \quad (5)$$

with value zero within the separator domain, where $\eta_i(x,t)$ represents the electrode overpotential, T is the cell temperature, assumed to be constant, R and F are the universal gas constant and the Faraday's constant, respectively. The intercalation exchange current density i_0 is defined as

$$i_{0,i} = k_i \sqrt{c_{e,i}(x,t) (c_{s,i}^{\text{max}} - c_{s,i}^*(x,t)) c_{s,i}^*(x,t)}, \quad (6)$$

where $c_{s,i}^{\max}$ is the maximum allowed concentration in each electrode, $c_{s,i}^*(x, t)$ denotes the Li-ions surface concentration, and k_i the kinetic reaction rate. The solid phase potential $\Phi_{s,i}(x, t)$ inside the two electrodes is modeled according to the Ohm's law

$$\frac{\partial}{\partial x} \left[\sigma_{\text{eff},i} \frac{\partial \Phi_{s,i}(x, t)}{\partial x} \right] = a_i F j_i(x, t), \quad (7)$$

where $\sigma_{\text{eff},i}$ is the electrodes effective conductivity

$$\sigma_{\text{eff},i} = \epsilon_i^p \sigma_i \quad (8)$$

with σ_i the electrodes conductivity. Similarly, Ohm's law is also used for the electrolytic potential $\Phi_{e,i}(x, t)$

$$a_i F j_i(x, t) + \frac{\partial}{\partial x} \left[\kappa_{\text{eff},i}(c_{e,i}(x, t)) \frac{\partial \Phi_{e,i}(x, t)}{\partial x} \right] = \frac{\partial}{\partial x} \left[\frac{2\kappa_{\text{eff},i}(c_{e,i}(x, t))RT}{F} (1 - t_+) \frac{\partial}{\partial x} \ln c_{e,i}(x, t) \right]. \quad (9)$$

In particular, $\kappa_{\text{eff},i}(c_{e,i}(x, t))$ is the effective conductivity of the liquid phase

$$\kappa_{\text{eff},i}(c_{e,i}(x, t)) = \epsilon_i^p \kappa(c_{e,i}(x, t)), \quad (10)$$

where $\kappa(c_{e,i}(x, t))$ is the electrolyte conductivity coefficient, assumed to be a polynomial function of the electrolyte concentration as in Lopez et al.⁸

$$\kappa(c_{e,i}(x, t)) = h_1 + h_2 s + h_3 s^2 + h_4 s^3 + h_5 s^4, \quad (11)$$

with $s = 10^{-3} c_{e,i}(x, t)$ and real coefficients $h_i, i = 1, \dots, 5$. Finally, the electrode overpotential is defined as follows

$$\eta_i(x, t) = \Phi_{s,i}(x, t) - \Phi_{e,i}(x, t) - U_i(\theta_i(x, t)), \quad (12)$$

where the open circuit potential of each electrode $U_i(\theta_i(x, t))$ is given by a nonlinear polynomial function of the surface stoichiometry $\theta_i(x, t) = \frac{c_{s,i}^*(x, t)}{c_i^{max}}$ as in Lopez et al.⁸

$$U_p(\theta_p) = f_1 + f_2 \tanh(f_3 \theta_p + f_4) + \frac{f_5}{(f_6 - \theta_p)^{f_7}} + f_5 f_8 + f_9 e^{f_{10} \theta_p^{f_{11}}} + f_{12} e^{f_{13}(\theta_p + f_{14})} \quad (13a)$$

$$U_n(\theta_n) = g_1 + g_2 e^{g_3 \theta_n} + g_4 e^{g_5 \theta_n}. \quad (13b)$$

The cell output voltage is given by

$$V_{out}(t) = \Phi_{s,p}(0_p, t) - \Phi_{s,n}(L_n, t). \quad (14)$$

The constants, the model parameters and the coefficients of U_p , U_n and κ_i are taken from Lopez et al.,⁸ except for the cathode diffusion coefficient $D_{s,p}$ and the electrolyte diffusion coefficient D_e which are taken from Ecker et al.⁶ In particular, the diffusion coefficients are chosen to better approximate real lithium-ion cell behavior. For more details about the P2D model and boundary conditions, the reader can refer to Ramadass et al.³¹ and Northrop et al.³² In the following, we rely on the numerical implementation of the P2D model provided by the freely available Li-ION Simulation BAttery Toolbox (*LIONSIMBA*⁴), using the parameters as discussed above.

3 Single particle model with electrolyte dynamics

The P2D model is a very detailed model, but also very complex to be used within the context of battery state estimation and control. For this reason, in the following model simplifications of the P2D are considered. The SPM¹⁸ has been used by many authors in the context of battery state estimation and control.^{22,33–35} The model is obtained from the P2D by approximating the solid phase of each electrode with a single spherical particle. Such particle presents an equivalent area equal to the one of the solid phase in the porous

electrode. In the SPM basic formulation, the diffusion of the electrolyte concentration and the thermal effects are assumed negligible. The diffusion of the ion concentration is approximated by its average along the x axis $\bar{c}_{s,i}(t, r_i)$, with the following equation

$$\frac{\partial \bar{c}_{s,i}(r, t)}{\partial t} = \frac{D_{s,i}}{r^2} \frac{\partial}{\partial r} \left(r^2 \frac{\partial \bar{c}_{s,i}(r, t)}{\partial r} \right). \quad (15)$$

The input current $I_{app}(t)$ enters the model in the Neumann boundary conditions

$$\left. \frac{\partial \bar{c}_{s,i}(r, t)}{\partial r} \right|_{r=0} = 0, \quad D_{s,i} \left. \frac{\partial \bar{c}_{s,i}(r, t)}{\partial r} \right|_{r=R_{p,i}} = -j_i, \quad (16)$$

where $j_p = -\frac{I_{app}(t)}{a_p L_p F A}$ and $j_n = \frac{I_{app}(t)}{a_n L_n F A}$. The initial condition is given by

$$\bar{c}_{s,i}(r, 0) = \bar{c}_{s,i}^0(r), \quad (17)$$

where $\bar{c}_{s,i}^0(r)$ is the initial concentration profile over the radial axis. Due to its simplicity, the SPM results particularly suitable for state estimation and control purposes. However, it shows inaccuracy for current greater than $0.5I_{1C}$, in particular in case of low electrolyte conductivity as discussed by Moura et al.²² In that work a single particle model with electrolyte dynamics (SPMe) is proposed in order to increase voltage prediction accuracy while maintaining the computational effort at a reasonable level. The same electrolyte diffusion equations as in Moura et al.²² are here adopted

$$\epsilon_p \frac{\partial c_{e,p}(x, t)}{\partial t} = D_{eff,p} \frac{\partial^2 c_{e,p}(x, t)}{\partial x^2} - \frac{1-t_+}{F A L_p} I_{app}(t) \quad (18a)$$

$$\epsilon_s \frac{\partial c_{e,s}(x, t)}{\partial t} = D_{eff,s} \frac{\partial^2 c_{e,s}(x, t)}{\partial x^2} \quad (18b)$$

$$\epsilon_n \frac{\partial c_{e,n}(x, t)}{\partial t} = D_{eff,n} \frac{\partial^2 c_{e,n}(x, t)}{\partial x^2} + \frac{1-t_+}{F A L_n} I_{app}(t) \quad (18c)$$

for $(x, t) \in (0, L) \times (0, T)$. The boundary conditions are given by

$$\frac{\partial c_{e,p}(0_p, t)}{\partial x} = \frac{\partial c_{e,n}(L_n, t)}{\partial x} = 0 \quad (19a)$$

$$D_{eff,p} \frac{\partial c_{e,p}(L_p, t)}{\partial x} = D_{eff,s} \frac{\partial c_{e,s}(0_s, t)}{\partial x} \quad (19b)$$

$$D_{eff,s} \frac{\partial c_{e,s}(L_s, t)}{\partial x} = D_{eff,n} \frac{\partial c_{e,n}(0_n, t)}{\partial x} \quad (19c)$$

and the initial condition is

$$c_{e,i}(x, 0) = c_{e,i}^0, \quad (20)$$

where $c_{e,i}^0$ is the initial electrolyte concentration in the layer i , with $i \in \{p, s, n\}$.

3.1 Further simplification of the SPM_e

In this section, the partial differential equation (15) which describes the lithium-ions diffusion in the solid phase is approximated by a set of Ordinary Differential Equations (ODEs). The solid diffusion dynamics can be reduced to a lower order system in several ways. In Bizeray et al.³⁶ the diffusion dynamic in the solid phase is spatially discretised using a Chebyshev orthogonal collocation method which enables fast and accurate simulations. In Subramanian et al.³⁷ the lithium concentration profile in the particles is approximated as a polynomial function (see Figure 1)

$$c_{s,i}(r, t) = a(t) + b(t) \frac{r^2}{R_{p,i}^2} + d(t) \frac{r^4}{R_{p,i}^4}, \quad (21)$$

where the coefficients $a(t)$, $b(t)$, $d(t)$ are expressed in terms of volume-averaged lithium concentration $\bar{c}_{s,i}^{avg}(t)$, volume-averaged concentration flux $q_i^{avg}(t)$ and surface concentration $\bar{c}_{s,i}^*(t)$. In this work, the model is simplified according to Subramanian et al.³⁷ and

Fick's law is reduced into a set of $N^{ode} = 4$ ODEs

$$\dot{\bar{c}}_{s,p}^{avg}(t) = \frac{3}{R_{p,p}FAL_p a_p} I_{app}(t) \quad (22a)$$

$$\dot{\bar{c}}_{s,n}^{avg}(t) = -\frac{3}{R_{p,n}FAL_n a_n} I_{app}(t) \quad (22b)$$

$$\dot{q}_p^{avg}(t) = -30 \frac{D_{s,p}}{R_{p,p}^2} q_p^{avg}(t) + \frac{45}{2R_{p,p}^2} \frac{1}{FAL_p a_p} I_{app}(t) \quad (22c)$$

$$\dot{q}_n^{avg}(t) = -30 \frac{D_{s,n}}{R_{p,n}^2} q_n^{avg}(t) - \frac{45}{2R_{p,n}^2} \frac{1}{FAL_n a_n} I_{app}(t). \quad (22d)$$

The positive and negative surface concentrations are then given by

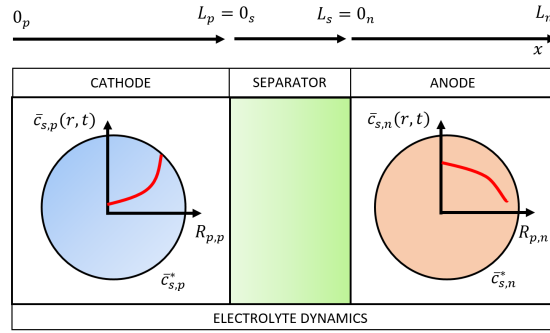


Figure 1: Schematic representation of the SPMe according to Subramanian et al. ³⁷

$$\bar{c}_{s,p}^*(t) = \bar{c}_{s,p}^{avg}(t) + \frac{8R_{p,p}}{35} q_p^{avg}(t) + \frac{R_{p,p}}{35D_{s,p}} \frac{1}{FAL_p a_p} I_{app}(t) \quad (23a)$$

$$\bar{c}_{s,n}^*(t) = \bar{c}_{s,n}^{avg}(t) + \frac{8R_{p,n}}{35} q_n^{avg}(t) - \frac{R_{p,n}}{35D_{s,n}} \frac{1}{FAL_n a_n} I_{app}(t). \quad (23b)$$

The output voltage is a nonlinear function of the states and the input

$$V(t) = U_p(\bar{\theta}_p(t)) - U_n(\bar{\theta}_n(t)) + \Delta\Phi_e(t) + \bar{\eta}_p(t) - \bar{\eta}_n(t), \quad (24)$$

where $\bar{\theta}_p(t)$ and $\bar{\theta}_n(t)$ are the positive and negative average surface stoichiometries, respectively given by

$$\bar{\theta}_p(t) = \frac{\bar{c}_{s,p}^*(t)}{c_p^{max}}, \quad \bar{\theta}_n(t) = \frac{\bar{c}_{s,n}^*(t)}{c_n^{max}}. \quad (25)$$

$\Delta\Phi_e(t)$ is the average electrolyte potential drop, which is approximated as

$$\Delta\Phi_e(t) = -\frac{I_{app}}{2A} \left(\frac{L_p}{\bar{\kappa}_{eff,p}} + \frac{2L_s}{\bar{\kappa}_{eff,s}} + \frac{L_n}{\bar{\kappa}_{eff,n}} \right) + \frac{2RT}{F} (1 - t_+) \ln \frac{c_e(0_p, t)}{c_e(0_n, t)}, \quad (26)$$

where $\bar{\kappa}_{eff,i}$ is the average effective electrolyte conductivity

$$\bar{\kappa}_{eff,i} = \epsilon_i^p \kappa(\bar{c}_{e,i}), \quad (27)$$

with $\bar{c}_{e,i} = \frac{1}{L_i} \int_{L_i} c_{e,i}(x, t) dx$ the average electrolyte concentration in layer i , with $i \in \{p, s, n\}$. Note that, differently from Moura et al.,²² in which the electrolyte conductivity is assumed uniform in the electrolyte concentration ($\kappa(c_e) \simeq \bar{\kappa}$), in this work we adopt a more realistic approximation. In particular, the effective electrolyte conductivity $\bar{\kappa}_{eff,i}$ is evaluated according to (27) using for each section the different average value of the electrolyte concentration $\bar{c}_{e,i}$. Finally, the positive and negative average overpotentials are given by

$$\bar{\eta}_p(t) = \beta \sinh^{-1} \left(\frac{-I_{app}(t)}{2AFL_p a_p \bar{i}_{0,p}(t)} \right) \quad (28a)$$

$$\bar{\eta}_n(t) = \beta \sinh^{-1} \left(\frac{I_{app}(t)}{2AFL_n a_n \bar{i}_{0,n}(t)} \right), \quad (28b)$$

where $\beta = \frac{2RT}{F}$ and

$$\bar{i}_{0,i}(t) = k_i \sqrt{\bar{c}_{e,i}(t) \bar{c}_{s,i}^*(t) (c_i^{max} - \bar{c}_{s,i}^*(t))}. \quad (29)$$

The obtained model consists of four ODEs and three Partial Differential Equations (PDEs). The PDEs are discretized using the finite-volume method described in Torchio et al.,⁴ where the spatial domain is divided into $3 \cdot N^{el}$ non-overlapping volumes with centered nodes, as shown in Figure 2 and $\bar{c}_{e,i}^k(t)$ is the volume average electrolyte concentration over the k -th volume.

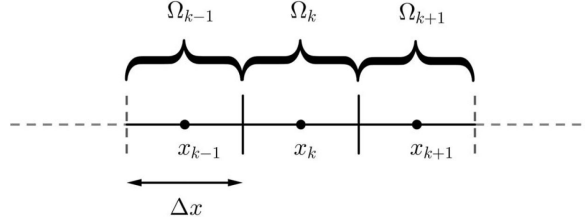


Figure 2: Finite volume discretization.

4 Optimal design of experiment and parameter estimation method

The value of the physical parameters of a lithium-ion cell varies significantly from cell to cell. This happens even when cells of the same chemistry and the same type are considered. In the context of state estimation and control, the model accuracy is fundamental in order to achieve high performance. For this reason, rather than using the mean values of the parameters distribution as in Ecker et al.,⁶ it is much better to resort to a parameters identification procedure. However, the use of standard identification current profiles (e.g. constant current, multistep discharging current) may not be sufficiently informative for this purpose. This has been shown in the context of lithium-ion batteries in, e.g. Lopez et al.,⁸ where the authors investigate the structural identifiability of the model parameter

vector $\phi \in \mathbb{R}^{N_\phi}$

$$\phi = [p \ t_+ \ D_e \ D_{s,p} \ D_{s,n} \ k_p \ k_n]^T. \quad (30)$$

when constant discharging currents are applied. The results underline that only a subset of the previous parameter vector is identifiable if the estimation process is based on voltage measurements only. In particular, the cathodic diffusion constant $D_{s,p}$ and the reaction rate constants (k_p, k_n) remain unidentifiable after multiple experiments. In this work we focus on the design of experiments to be conducted on a Li-ion cell in order to estimate the same parameter vector ϕ as in Lopez et al. ⁸ The objective is to find an optimal input current profile aiming to maximize the accuracy of the vector ϕ . We consider ϕ^* as the true value of the parameter vector and ϕ_0 as the initial guess of the parameter estimation procedure (see Table 1). Note that, ϕ_0 has been set equal to the most probable value of the parameters.

Table 1: Initial guess and true value of the parameters to be estimated.

Parameter	Unit	Description	Initial guess ϕ_0	True value ϕ^*
p	-	Bruggeman coefficient	1.6613	1.5
t_+	-	Cationic transference number	0.4975	0.363
D_e ⁶	m^2s^{-1}	Diffusion coefficient in the electrolyte	$1.3376 \cdot 10^{-10}$	$2.44 \cdot 10^{-10}$
$D_{s,p}$ ⁶	m^2s^{-1}	Diffusion coefficient in the cathode	$7.98 \cdot 10^{-11}$	$7.5 \cdot 10^{-11}$
$D_{s,n}$	m^2s^{-1}	Diffusion coefficient in the anode	$1.17 \cdot 10^{-13}$	10^{-13}
k_p	$\text{m}^{2.5}\text{mol}^{-0.5}\text{s}^{-1}$	Kinetic reaction rate constant in the cathode	$1.8266 \cdot 10^{-11}$	$2 \cdot 10^{-11}$
k_n	$\text{m}^{2.5}\text{mol}^{-0.5}\text{s}^{-1}$	Kinetic reaction rate constant in the anode	$1.4769 \cdot 10^{-11}$	$2 \cdot 10^{-11}$

The set of ODEs and nonlinear output equation describing the SPMc can be expressed as

$$\dot{x}(t) = f(x(t), u(t), \phi) \quad (31a)$$

$$y(t) = g(x(t), u(t), \phi) \quad (31b)$$

$$x(t_0) = x_0, \quad (31c)$$

where the model input $u(t) \in \mathbb{R}$ is the applied current $I_{app}(t)$, the model output $y(t) \in \mathbb{R}$ is the voltage $V(t)$ and the differential state vector $x(t) \in \mathbb{R}^m$, with $m = N^{ode} + 3 \cdot N^{el}$, is given by

$$x = [\bar{c}_{s,p}^{avg} \quad \bar{c}_{s,n}^{avg} \quad q_p^{avg} \quad q_n^{avg} \quad x_{\bar{c}_e}]^T, \quad (32)$$

where

$$x_{\bar{c}_e} = [\bar{c}_{e,p}^1 \quad \dots \quad \bar{c}_{e,p}^{N^{el}} \quad \bar{c}_{e,s}^1 \quad \dots \quad \bar{c}_{e,s}^{N^{el}} \quad \bar{c}_{e,n}^1 \quad \dots \quad \bar{c}_{e,n}^{N^{el}}]^T. \quad (33)$$

Moreover, $\phi \in \mathbb{R}^{N_\phi}$ is the set of parameters we aim to estimate, $t_0 \in \mathbb{R}^+$ is the initial time and $x_0 \in \mathbb{R}^m$ is the initial state vector. In the following, we assume that both inputs and outputs are applied/measured every t_s seconds. Let $\mathbf{u}^{\tilde{\zeta}} \in \mathbb{R}^N$ denote the input sequence for a given experiment $\tilde{\zeta}$ over a time interval $[t_i^{\tilde{\zeta}}, t_f^{\tilde{\zeta}}]$

$$\mathbf{u}^{\tilde{\zeta}} = [u(t_i^{\tilde{\zeta}}), u(t_i^{\tilde{\zeta}} + t_s), \dots, u(t_f^{\tilde{\zeta}})]^T, \quad (34)$$

where the number of control inputs and acquired outputs is $N = \frac{t_f^{\tilde{\zeta}} - t_i^{\tilde{\zeta}}}{t_s}$. Note that the sequence $\mathbf{u}^{\tilde{\zeta}}$ corresponds to a piecewise constant input. Let $\mathbf{y}^{\tilde{\zeta}}(\phi) \in \mathbb{R}^N$ be the output sequence corresponding to the application of the input sequence $\mathbf{u}^{\tilde{\zeta}}$ for the given experiment $\tilde{\zeta}$, that is

$$\mathbf{y}^{\tilde{\zeta}} = [y(t_i^{\tilde{\zeta}}), y(t_i^{\tilde{\zeta}} + t_s), \dots, y(t_f^{\tilde{\zeta}})]^T. \quad (35)$$

In the following, the output measurements are assumed to be affected by zero mean Gaussian noise, uncorrelated over time. In particular, for the true value of the parameter

vector ϕ^* , one has

$$\bar{y}(t) = g(x(t), u(t), \phi^*) + v(t), \quad (36)$$

where $v(t) \sim \mathcal{N}(0, \sigma_y^2)$. The vector of the noisy observed data $\bar{\mathbf{y}}^\xi \in \mathbb{R}^N$ is defined as follows

$$\bar{\mathbf{y}}^\xi = [\bar{y}(t_i^\xi), \dots, \bar{y}(t_f^\xi)]. \quad (37)$$

It holds that $\bar{\mathbf{y}}^\xi \sim \mathcal{N}(\mathbf{y}^\xi(\phi^*), C_y)$, where $C_y \in \mathbb{R}^{N \times N}$ is the measurement covariance matrix. In particular, C_y is a diagonal matrix with entries given by the measurement error variances σ_y^2 , i.e.

$$C_y = \sigma_y^2 \mathbb{I}_N, \quad (38)$$

where \mathbb{I}_N is the identity matrix of order N .

4.1 Structural identifiability, sensitivity matrix and ill-conditioning analysis

The analysis of ill-conditioning sources in the parameter sensitivity matrix allows to assess the structural identifiability of model parameters.^{38,39} The sensitivity matrix for a given experiment ξ is given by the Jacobian matrix of the output vector $\mathbf{y}^\xi(\phi)$ with respect to the parameters we aim to estimate, i.e.

$$S^\xi(\phi) = \nabla_\phi \mathbf{y}^\xi(\phi), \quad (39)$$

with $S^\xi(\phi) \in \mathbb{R}^{N \times N_\phi}$. Note that, the sensitivity matrix is not related to measurement data and measurement noise, but depends only on the model equations, on the input vector (i.e.

the experiment) and on the parameter vector ϕ in which it is evaluated. For this reason, it is possible to compute the sensitivity matrix for a particular experiment ξ directly in simulation. In the following, the Jacobian matrix of the output vector with respect to the parameters, i.e. the sensitivity matrix, is numerically computed using the finite difference method. This provides a useful approximation for the columns of the sensitivity matrix, given as follows

$$S_j^\xi = \frac{\mathbf{y}^\xi(\{\phi^1, \dots, \phi^i + h, \dots, \phi^{N_\phi}\}) - \mathbf{y}^\xi(\phi)}{h}, \quad j = 1, 2, \dots, N_\phi, \quad (40)$$

where h is suitably chosen (in the following $h = 0.001$). This choice is motivated by the fact that the evaluation of the analytical expression of $S^\xi(\phi)$ becomes prohibitive in case of large dimensions of the output sequence, that is required especially for long horizons problems.

The finite difference approach in the context of sensitivity analysis is also suggested in the guideline of *CasADi*,⁴⁰ the toolbox we will adopt for optimization purposes (see Sec. 4.3).

The ill-conditioning of $S^\xi(\phi)$ implies that one or more parameters are unidentifiable for a given experiment ξ . This can be assessed by analyzing the singular values $\zeta_1 \dots \zeta_{N_\phi}$ of the sensitivity matrix,^{8,41,42} which are computed with the singular value decomposition method.⁴³ In particular, we consider the condition number

$$\kappa(S^\xi(\phi)) = \frac{\zeta^{max}}{\zeta^{min}} \quad (41)$$

and the collinearity index

$$\gamma(S^\xi(\phi)) = \frac{1}{\zeta^{min}}. \quad (42)$$

where ζ^{max} and ζ^{min} are the maximum and the minimum singular value of the sensitivity

matrix $S^\zeta(\phi)$. High values of the condition number and of the collinearity index indicate that the sensitivity matrix is ill-conditioned.

4.2 Fisher information matrix and covariance of the parameters

Once the experiment ζ is performed and the output measurement sequence $\bar{\mathbf{y}}^\zeta$ is collected, the parameters are estimated by solving the following maximum likelihood problem

$$\hat{\phi} = \arg \min_{\phi \in [\phi_m, \phi_M]} \left[(\bar{\mathbf{y}}^\zeta - \mathbf{y}^\zeta(\phi))^T (\bar{\mathbf{y}}^\zeta - \mathbf{y}^\zeta(\phi)) \right], \quad (43)$$

where ϕ_m and ϕ_M are suitable lower and upper bound that restrict the feasible region of the optimization problem to a set that is physically meaningful. Due to the fact that $\bar{\mathbf{y}}^\zeta$ is a random variable, one has that also the estimated parameter vector $\hat{\phi}$ is a random variable, i.e. $\hat{\phi} \sim \mathcal{N}(\phi^*, C_\phi^\zeta)$. Let $C_\phi^\zeta \in \mathbb{R}^{N_\phi \times N_\phi}$ denotes the covariance matrix of the parameters, that depends on the experiment ζ . The design of experiment proposed in the following aims to reduce such covariance. In particular, we rely on the Fisher Information Matrix,⁹ denoted by $F^\zeta(\phi) \in \mathbb{R}^{N_\phi \times N_\phi}$, that is a symmetric matrix giving a measure of how much an experiment is informative and it is given by

$$F^\zeta(\phi) = S^\zeta(\phi)^T C_y^{-1} S^\zeta(\phi), \quad (44)$$

The generalized inverse of the Fisher Information Matrix gives a lower bound for the parameter covariance matrix according to the Cramer-Rao bound⁴⁴

$$F^\zeta(\phi)^{-1} \leq C_\phi^\zeta. \quad (45)$$

The Fisher Information Matrix for a nonlinear system is strictly dependent on the value of the parameter vector ϕ in which it is evaluated, as for the sensitivity matrix. Note that, by applying in simulation a standard Constant Current (CC) discharging protocol to the

SPMe, the resulting sensitivity matrix $S^{\tilde{\zeta}}(\phi)$ is full rank. This result is promising because implies that there exists an input sequence for which the Fisher matrix is positive definite and therefore its inverse matrix is well defined.

4.3 Optimization method

In this section, an iterative optimal design of experiment method is described. In particular, a sequence of experiments $\tilde{\zeta}_i, i = 1, \dots, n$ is designed in order to estimate the parameter vector $\hat{\phi}$ with high accuracy and maximal statistical reliability.³⁰ At each iteration, the experiment $\tilde{\zeta}_i$ is obtained by minimizing a functional of the parameter covariance matrix $J\left(C_{\hat{\phi}_{i-1}}^{\tilde{\zeta}_i}\right)$, i.e. by solving the following constrained optimization problem

$$\min_{\mathbf{u}^{\tilde{\zeta}_i}} J\left(C_{\hat{\phi}_{i-1}}^{\tilde{\zeta}_i}\right), \quad (46)$$

subject to

$$\text{model dynamics} \quad (47a)$$

$$x(t_i^{\tilde{\zeta}_i}) = x_0^{\tilde{\zeta}_i} \quad (47b)$$

$$-I_{\max} \leq u(t) \leq I_{\max} \quad (47c)$$

$$h(x(t), u(t), \hat{\phi}_{i-1}) \leq 0, \quad (47d)$$

where I_{\max} is a suitable bound for the input and $x_0^{\tilde{\zeta}_i}$ is the initial state for the experiment $\tilde{\zeta}_i$. Since it is not possible to minimize directly the variance of the parameters, several optimization criteria can be used. In the formulation of problem (46) we rely on the A-criterion,⁴⁵ i.e. on the minimization of the trace of the approximated covariance matrix

$$J\left(C_{\hat{\phi}_{i-1}}^{\tilde{\zeta}_i}\right) = \text{Tr}\left(C_{\hat{\phi}_{i-1}}^{\tilde{\zeta}_i}\right) \quad (48)$$

The resulting input \mathbf{u}^{ζ_i} , obtained by solving the above optimization problem, is applied to the model. Subsequently, the estimated parameter vector is updated with $\hat{\phi}_i$, obtained as the solution of the maximum likelihood estimation process (43) using the output measurements collected during all the experiments ζ_1, \dots, ζ_i performed so far. A schematic representation of the method is resumed in Figure 3. Voltage and state of charge con-

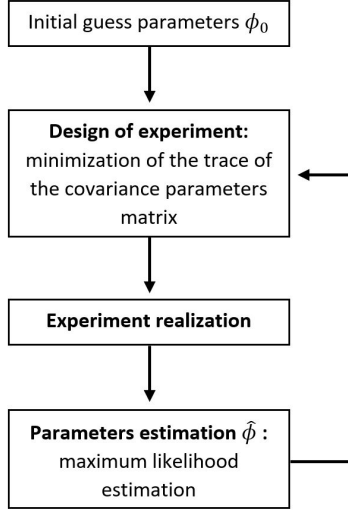


Figure 3: Schematic representation of the optimal experimental design and parameters estimation process.

straints are taken into account using the nonlinear constraint in (47d), that allows to explicitly consider safety during the experiments realization. In order to guarantee that each experiment has the same initial state, i.e. $x_0^{\zeta_i} = x_0$, a charging procedure, followed by a resting period which brings the system to a steady state, is applied to the cell before each new experiment. The maximum likelihood problem in (43) as well as the nonlinear optimization problem in (46) have been solved using the interior point method^{46–48} and *CasADi*,⁴⁰ an open source tool which provides a symbolic framework for nonlinear numerical optimization algorithms. Furthermore, the solver efficiency has been improved by performing a scaling procedure to the parameters in Table 1 over their nominal values (ϕ^*), which may vary among several orders of magnitude.³⁰ In real battery experiments,

the parameters should be scaled considering their likely values, which are indicated on the cell data-sheet.

4.4 Computational cost reduction by sub-optimal approach

Since the objective of each experiment is to lead to a covariance parameter matrix low enough to guarantee a meaningful parameter estimation, the input may need to be optimized over a long experimental time. This, together with the nonlinearities of the model, could increase dramatically the computational burden of problem (46). For this reason, we divide the design of the experiment $\tilde{\zeta}_i$ into M sub-problems, each involving only a fraction of the overall set of optimization variables, as shown in Fig. 4. Each step aims to design the

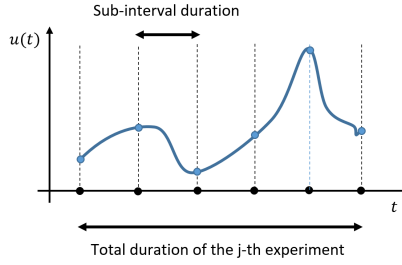


Figure 4: Schematic representation of the sub-optimal experimental design.

input vector $\mathbf{u}^{\tilde{\zeta}_{i,j}} \in \mathcal{R}^{\tilde{N}}$, $j = 1, \dots, M$, over the time interval $[t_i^{\tilde{\zeta}_{i,j}}, t_f^{\tilde{\zeta}_{i,j}}]$, where $\tilde{N} = \frac{t_f^{\tilde{\zeta}_{i,j}} - t_i^{\tilde{\zeta}_{i,j}}}{t_s}$, i.e. $\tilde{N} = \frac{N}{M}$. At the j -th step, the input $\mathbf{u}^{\tilde{\zeta}_{i,j}}$ is designed by minimizing the trace of $\mathbf{C}_{\phi}^{\left[\tilde{\zeta}_{i,1} \dots \tilde{\zeta}_{i,j}\right]}$, that is the covariance matrix over the $1, \dots, j$ partial experiments performed so far in simulation. In particular, at each step the following constrained optimization problem is solved

$$\min_{\mathbf{u}^{\tilde{\zeta}_{i,j}}} \text{Tr} \left(\mathbf{C}_{\phi_{i-1}}^{\left[\tilde{\zeta}_{i,1} \dots \tilde{\zeta}_{i,j}\right]} \right) \quad (49)$$

subject to

$$\text{model dynamics} \quad (50a)$$

$$x(t_i^{\xi_{i,j}}) = x_0^{\xi_{i,j}} \quad (50b)$$

$$-I_{\max} \leq u(t) \leq I_{\max} \quad (50c)$$

$$h(x(t), u(t), \hat{\phi}_{i-1}) \leq 0 \quad (50d)$$

The different subproblems are solved in sequence, $j = 1, \dots, M$ and for each $j = 2, \dots, M$, the initial condition is obtained by simulating the effect of the input designed so far on the SPMc starting with initial condition x_0 . Once all the M steps have been performed, one obtains a sub-optimal input sequence, given by

$$\tilde{\mathbf{u}}^{\xi_i} = \left[\mathbf{u}^{\xi_{i,1}}, \mathbf{u}^{\xi_{i,2}}, \dots, \mathbf{u}^{\xi_{i,M}} \right]. \quad (51)$$

Only at this point the sequence $\tilde{\mathbf{u}}^{\xi_i}$ is applied to the system and the result of the experiment ξ_i is then obtained. Finally, $\hat{\phi}_i$ is estimated solving (43). The sub-optimality comes from the division of the DoE into M sub-problems, which was required for reducing the complexity of the optimization problem. Thanks to this scheme, it is possible to consider long experiments, useful for achieving low covariance of the parameters, without dramatically increasing the computational burden. The optimal input design process ends when one of the following conditions is satisfied:

- a variance threshold is achieved;
- a maximum numbers of experiments has been executed;
- no more significant covariance decrease is obtained.

This allows us to estimate the parameter vector $\hat{\phi}_i$ with high accuracy, while maintaining the computational burden at a reasonable level. In Algorithm 1 the main features of the

sub-optimal approach are resumed.

Algorithm 1 Sub-optimal design of experiment ζ_i .

- 1: Initialize the time: $t_i^{\zeta_i,1} = t_i^{\zeta_i}$
 - 2: Initialize the state: $x_0^{\zeta_i,1} = x_0^{\zeta_i}$
 - 3: **for** $j = 1$ **to** M **do**
 - 4: Compute the input by solving the optimization problem (49)
 - 5: Update the time: $t_i^{\zeta_i,j+1} = t_i^{\zeta_i,j} + \frac{t_f^{\zeta_i} - t_i^{\zeta_i}}{M}$
 - 6: Update the state applying the input sequence computed so far to the SPMe in simulation:

$$x_0^{\zeta_i,j+1} = x \left(t_i^{\zeta_i,j} + \frac{(t_f^{\zeta_i} - t_i^{\zeta_i})}{M} \right)$$
 - 7: **end for**
 - 8: Concatenate the sub-problems solutions in order to obtain the input sequence of the experiment ζ_i :
 $\mathbf{u}^{\zeta_i} = [\mathbf{u}^{\zeta_i,1} \dots \mathbf{u}^{\zeta_i,M}]$
 - 9: Update the estimated parameter vector:
 $\hat{\phi}_i = \arg \min [(\bar{\mathbf{y}}^{\zeta_i} - \mathbf{y}^{\zeta_i}(\phi_i))^T (\bar{\mathbf{y}}^{\zeta_i} - \mathbf{y}^{\zeta_i}(\phi_i))],$
 where $\phi_i \in [\phi_m, \phi_M]$
-

In Table 2 the sub-optimal approach is compared with the optimal one which relies on the numerical solution of the optimization problem in (46) over the whole time horizon $t_f^{\zeta_i} - t_i^{\zeta_i}$. The simulation is performed for $M = 4$, $t_f^{\zeta_i} - t_i^{\zeta_i} = 200$ s, $t_s = 5$ s and $\hat{\phi}_{i-1} = \phi_0$. In particular, the two approaches are compared in terms of computational time and trace of the covariance matrix. As it can be noticed, the sub-optimal approach presents a significant burden reduction while achieving high parameters accuracy.

Table 2: Comparison between the performances of the optimal and the sub-optimal design process.

Optimization method	Computational time [s]	Scaled Tr $\left(C_{\phi}^{\zeta} \right)$
Optimal	68.51	0.020
Sub-optimal	18.30	0.025

5 Optimal DoE applied to SPM_e

In this section, the optimal DoE described in Sec. 4 is applied to the SPM_e, assuming this latter to be the real plant and a comparison with standard identification methods (CC and multistep discharging profiles) is shown. A zero mean Gaussian measurement noise of $0.3mV$ is considered, with a corresponding variance of $\sigma_y^2 = 0.09 \cdot 10^{-6}$. Such noise is chosen to be consistent with the precision of the mostly used experimental instruments. In the following, the output is sampled with $t_s = 5s$. All the proposed approaches have the same initial condition x_0 is

$$x_0 = [3900 \ 14870 \ 0 \ 0 \ 2000 \ \dots \ 2000 \ \dots \ 2000]. \quad (52)$$

5.1 Optimal design approach

The proposed method is based on a sequence of experiments ζ_i , $i = 1, \dots, n$, each with duration $t_f^{\zeta_i} - t_i^{\zeta_i} = 1000s$ subdivided, for computational reasons, into $M = 4$ sub-optimal steps (Algorithm 1). The optimal input sequence is piece-wise constant over each $t_s = 5s$. In the following, the performance of the optimal DoE are evaluated in terms of convergence of the estimated parameter vector to the true value and variances reduction over $n = 10$ experiments. All the experiments present the same duration and initial condition. After each experiment, in order to bring the initial condition back to x_0 ($x_0^{\zeta_i} = x_0$, $i = 1, \dots, n$), a CC charging current of $1C$, followed by a resting period of $T_{rest} = 400s$, is applied. The input sequence of the optimal DoE is obtained as described in Sec. 4.4, with

$$-I_{\max} \leq u(t) \leq I_{\max} \quad (53a)$$

$$V_{\min} \leq y(t) \leq V_{\max}, \quad (53b)$$

where $I_{\max} = 1C$, $V_{\min} = 2.5V$ and $V_{\max} = 4.35V$.

5.2 CC discharging approach

The CC discharging approach is based on a sequence of experiments ξ_i , $i = 1, \dots, n$, with $n = 10$, each of them consisting of a simple constant current discharging protocol with 1C and time duration 1000s. Also in this case, at the beginning of each experiment, the initial condition is brought back to x_0 ($x_0^{\xi_i} = x_0$, $i = 1, \dots, n$) by applying a CC charging current of 1C, followed by a resting period of $T_{rest} = 400$ s. Fig. 5 reports the current and voltage profiles obtained with the optimal DoE and the CC discharging approach.

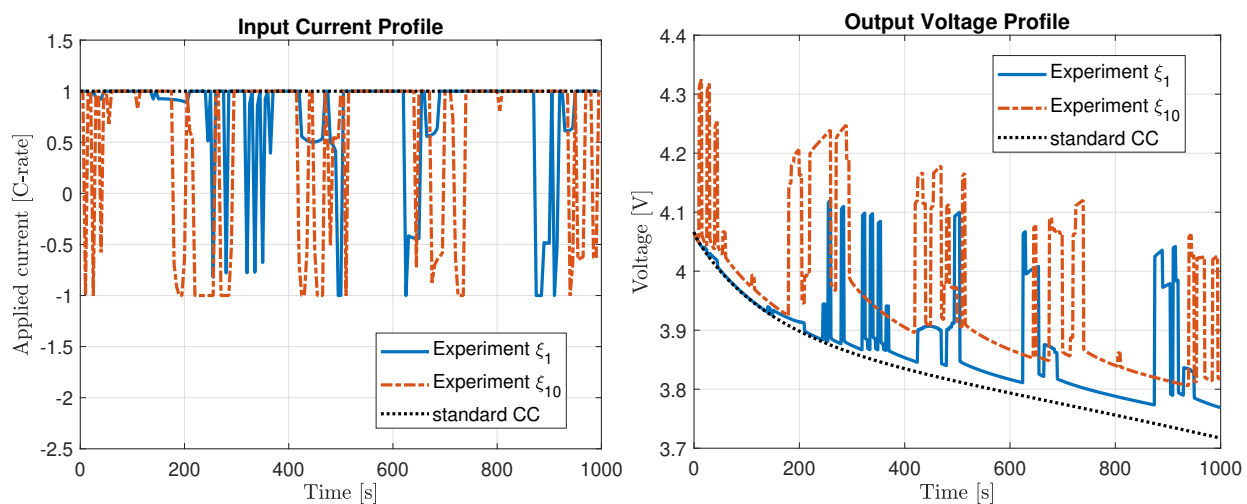


Figure 5: Current input profile and voltage output response applied during the optimal DoE.

5.3 Multistep discharging approach

The multiple step discharging current profile explores the whole battery state of charge range, as described in Fig. 6. In particular, the battery is discharged from 100% of state of charge in 5 steps. Each step applies a 1C current for 600s followed by 1400s of rest. Differently from the previous approaches the multistep discharging protocol consists of a single experiment of time duration 10000s. As it can be noticed the overall duration of all the approaches is the same (10000s).

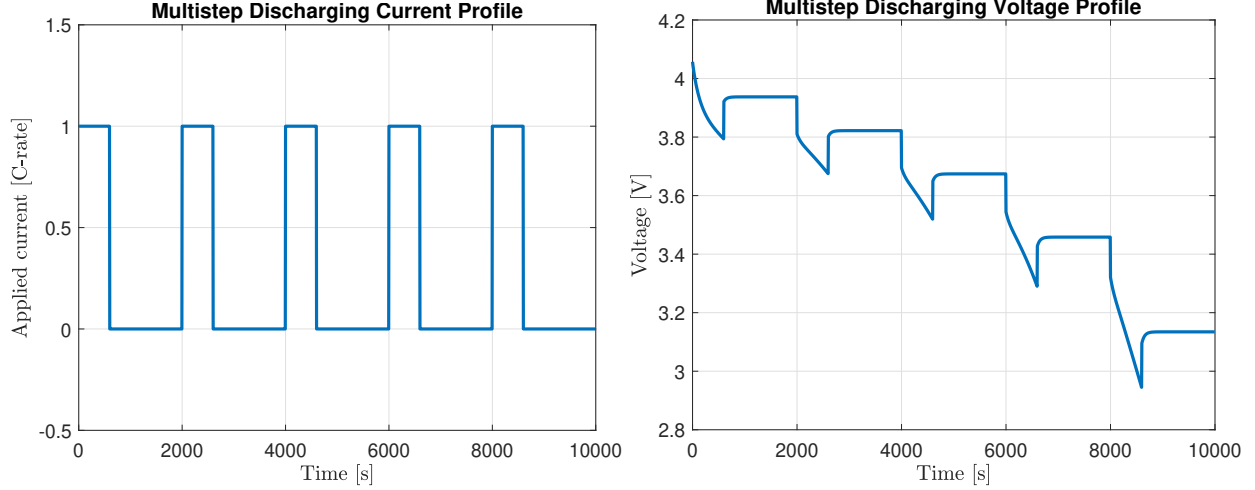


Figure 6: Current and voltage profiles used for multistep discharge identification.

5.4 Results comparison

In Figure 7, the experimental procedures are compared in terms of convergence of the scaled estimated parameter vector $\hat{\phi}$ to the true values ϕ^* , i.e. in terms of the euclidean norm

$$\|\hat{\phi} - \phi^*\| = \sqrt{(\hat{\phi} - \phi^*)^T (\hat{\phi} - \phi^*)}. \tag{54}$$

As it can be noticed, the parameter vector identified using the optimal DoE presents a fast convergence to the real value and a very low error even after the first experiment (1000s). On the other side, standard approaches require a longer time to reduce the gap between the identified parameter vector and the true one. Figure 8 highlights how the different SPMs scaled parameters convergence to their true values using the optimal DoE approach.

Table 3 shows the parameter vector estimated after the last experiment for all the approaches. In particular, the optimal DoE results the most accurate, although all the approaches show low estimation error at the end of the experimental procedure. Note that, thanks to the behavior shown in Figure 7, the optimal DoE already guarantees

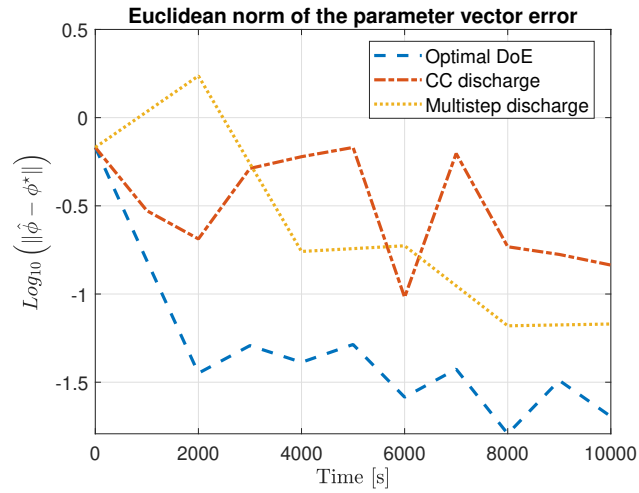


Figure 7: Comparison between the optimal experimental approach and the standard ones in terms of Euclidean distance of the parameter vector to the true value.

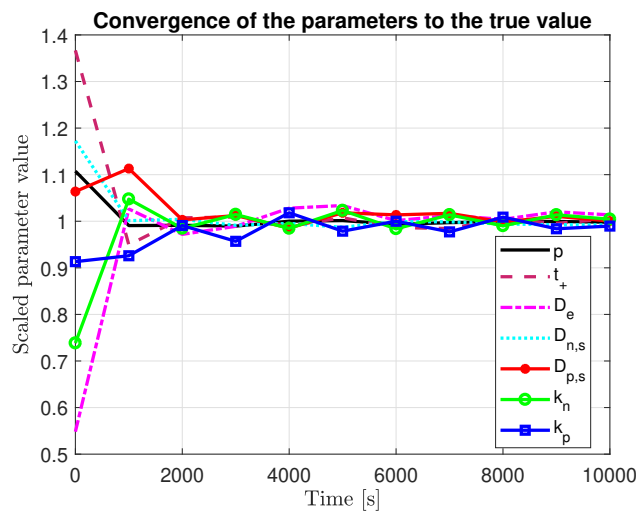


Figure 8: Convergence of the parameters to the true values.

low estimation error after 1000s. Considering the indexes introduced in Sec. 4.1 one

Table 3: Identified scaled parameters at the end of the experiment procedure using both optimal and standard approaches compared with the initial guess and the true value.

Parameter	ϕ_0	ϕ^*	$\hat{\phi}_{DoE}$	$\hat{\phi}_{CC}$	$\hat{\phi}_{m-step}$
p	1.1075	1	0.9979	1.0105	0.9911
t_+	1.3668	1	1.0052	0.9944	0.9579
D_e	0.5482	1	1.0136	1.0975	0.9990
$D_{s,p}$	1.1724	1	0.9920	0.9707	1.0029
$D_{s,n}$	1.0638	1	1.0004	1.0192	1.0498
k_p	0.7385	1	1.0044	1.0866	0.9903
k_n	0.9133	1	0.9896	0.9460	0.9885

can evaluate the presence of ill-conditioning sources and unidentifiable parameters. In particular, the value of such indexes after the last experiment are reported in Table 4. As it can be noticed, the collinearity index and the condition number are higher using the CC discharging approach than the optimal DoE and the multistep. This implies that, using the CC discharging approach, some parameters may remain unidentifiable after the last experiment. Note that, thanks to the behavior shown in Figure 7, with the optimal DoE these indexes were already significantly low after 1000s. Finally, in Table 5 shows

Table 4: Condition number and collinearity index at the end of the experimental realization.

Index	Optimal DoE	Standard	Multistep discharge
κ	577	31963	260
γ	152	7548	110

the variance reduction during the experiments realization. In particular it emerges that the variance of all the parameters in the optimal DoE is very low already after the first experiment (1000s), while the multistep discharging approach requires 10000s to achieve

high performance. In the CC discharging method the parameter variance still remains high at the last experiment. These results are promising since they underline that an optimal design of experiment can significantly improve parameters estimation accuracy (both in terms of converging parameter values and variance). Furthermore, the number of experiments required for the convergence of the parameters to the true values, i.e. the time-duration of the experimental realization required for an accurate identification, is much shorter using the optimal DoE than the standard current profiles.

Table 5: Comparison between scaled parameter variances during the identification process, both in case of optimal design of experiment and standard approach.

Parameter	Variance after ζ_1			Variance after ζ_{10}		
	Optimal DoE	CC discharge	Multistep discharge	Optimal DoE	CC discharge	Multistep discharge
p	$5 \cdot 10^{-5}$	1.21	0.0636	10^{-5}	0.24	10^{-4}
t_+	$8 \cdot 10^{-4}$	0.92	0.0225	$1.6 \cdot 10^{-4}$	0.19	$4 \cdot 10^{-4}$
D_e	$6 \cdot 10^{-3}$	6.97	0.5488	$1.2 \cdot 10^{-3}$	1.39	$6 \cdot 10^{-4}$
$D_{s,p}$	$6 \cdot 10^{-4}$	0.59	0.038	10^{-4}	0.12	10^{-5}
$D_{s,n}$	$9 \cdot 10^{-4}$	0.01	0.0166	$1.86 \cdot 10^{-4}$	$2.9 \cdot 10^{-3}$	$5 \cdot 10^{-4}$
k_p	$1.5 \cdot 10^{-3}$	14.88	0.8118	$3 \cdot 10^{-4}$	2.98	10^{-4}
k_n	$2.5 \cdot 10^{-3}$	1.10	0.1004	$4.9 \cdot 10^{-4}$	0.22	10^{-4}

The average time needed to solve the optimization problem described in Sec. 4.4 and compute the current profile for a single experiment is 520.81 s, while the average time needed to solve identification process in (43) is 13.59 s. The simulations are performed on a Windows 10 machine with 16Gbytes of RAM and Intel core I7-6700HK quad core processor 3.5 GHz. Note that, since the design of experiment and the parameter estimation process can be conducted offline, the time required by the proposed method appears suitable for real applications.

6 Optimal DoE applied to P2D model

In the section above, the optimal DoE has been conducted on the SPMe, assuming that the model used as the real plant and the one used for the parameters estimation were the

same. For this reason, the measurement data has been collected by simulating the SPMe output affected by a zero mean gaussian error. However, while the SPMe is particularly suitable for control purposes, its use for accurately simulating a real lithium-ion cell may be inadequate. For this reason, in the following, LIONSIMBA, a battery simulator which implements the P2D model, is assumed to be the real plant, with the output voltage affected by a zero mean gaussian error of $0.3mV$, with variance $\sigma_y = 0.09^{-6}$. It is important to notice that the use of two models, a model for simulation (very detailed) and a model for control (simpler), is a well known procedure. In particular, this allows to assess, in a preliminary way, the practical effectiveness of a novel control approach thus reducing time and costs during the experimental phase.

In the following, we assign value ϕ^* (see Table 1) to the parameters of the P2D. Note that, in general, the parameter vector resulting from the optimization may be different from ϕ^* . In fact, although physically meaningful, the use of a simplified model with parameter values equal to the ones of the real plant (P2D) may not be the best choice in terms of output fitting. In particular, the SPMe implementation with the parameter vector ϕ^* presents an RMS error in the voltage prediction of the P2D during normal cycling around few mV . This lack of accuracy comes in the form of a bias, and, although this could seem negligible, such error may cause problems in the context of state estimation. In the following, the parameters of the SPMe with the best fitting in terms of voltage are considered unknown, as in real experiments, and the parameter vector ϕ^* in Table 3 is used only to simulate for comparative purposes the SPMe with the P2D parameters. Furthermore, the optimal DoE is compared with standard experimental approaches, such as CC and multistep discharging protocols. The experimental setting adopted is the same of Sec. 5. The experiments are performed on LIONSIMBA⁴). Figure 9 shows the Euclidean distance between the estimated parameter vector $\hat{\phi}$ and ϕ^* . As discussed above, such distance is not expected to go to zero, since it is not guaranteed that the best fit will come with ϕ^* . However, a low value of this Euclidean norm ensures a physical meaning of the

estimated parameters. Note that, in real experiments the true parameters are unknown but we can evaluate the model performance in terms of output fitting of validation data and in terms of closedness to the data-sheet parameters. As it can be noticed from Figure 9, the parameter vector identified with the optimal DoE is closer to the one of the P2D model than in the standard approaches. Table 6 shows the parameters estimated after the last

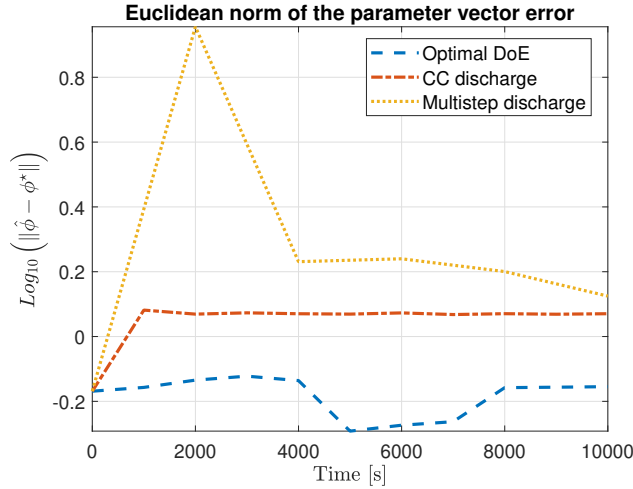


Figure 9: Comparison between the optimal DoE and the standard approach, experimentally applied to *LIONSIMBA*.

experiment for all the approaches. In this case, many parameters such as the Bruggeman coefficient (using the CC discharging approach) and the electrolyte diffusion coefficient (using the multistep discharging approach) seem losing their physical meaning (in bold, in Table 6), while the optimal DoE allows to identify parameters close to the nominal value.

6.1 Validation of the SPMe with the identified parameters

In this section, the SPMe is validated, in terms of P2D voltage prediction, using the parameters identified in the section above with the optimal DoE and the standard approaches. Furthermore, the comparison with the SPMe using ϕ^* is shown. In particular, the current input profile $u_{val}(t)$ used for the validation (Figure 10) consists of a biased multi-sinusoidal current with frequency $f_1 = 20$ mHz and $f_2 = 5$ mHz, $I_{bias} = 0.5$ C as mean value and

Table 6: Identified scaled parameter of the SPM_e after 10 experiments conducted on the P2D model.

Parameter	ϕ^*	$\hat{\phi}_{DoE}$	$\hat{\phi}_{cc}$	$\hat{\phi}_{m-step}$
p	1	0.6150	0.1000	0.8776
t_+	1	0.9472	0.8537	0.8905
D_e	1	0.4478	0.4303	2.2264
$D_{s,p}$	1	1.1164	0.8236	0.8508
$D_{s,n}$	1	0.9065	0.7288	0.7400
k_p	1	1.0011	0.7331	1.3804
k_n	1	0.8897	0.7742	1.1032

$I_{sin} = 0.25$ C as peak value of the sinusoidal components

$$u_{val}(t) = I_{sin} (\sin(2\pi f_1 t) + \sin(2\pi f_2 t)) + I_{bias}. \quad (55)$$

The results of the validation process are shown in Figure 11. This latter reports the

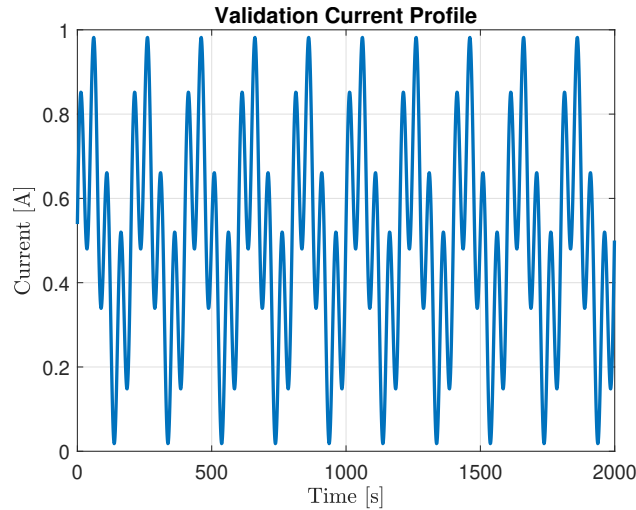


Figure 10: Input current profile used for validation.

evolution of the voltage RMS error between the SPM_e and the P2D, evaluated after each experiment on the validation profile. As it can be noticed, the RMS error using the optimal

DoE is very low after the first experiment, while the standard approaches present a slow convergence to an higher error. Note that, all the estimation methods improve the accuracy in the P2D voltage prediction given by the SPMe with ϕ^* . On the other side, the optimal DoE is the one which provides physically meaningful parameters in the shortest time.

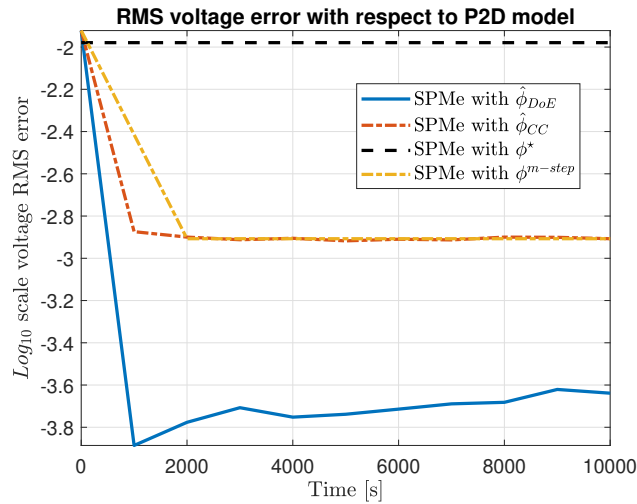


Figure 11: Comparison between the optimal experimental approach and the standard ones in terms of root mean square error.

The validation performed so far shows promising results in the application of the optimal DoE to the P2D model, used in this context as the real plant. In particular, it is demonstrated that the estimation of the SPMe parameters according to the optimal DoE can significantly increase the model performance in the P2D voltage prediction.

7 Conclusion

The use of accurate models in advanced BMSs is necessary in order to achieve high performance in battery operations. For this reason, a suitable identification process is required. Note that, the input signal has to be sufficiently exciting during the experiment realization, in order to reduce parameters uncertainty. In this work, the optimal DoE is applied to the SPMe, so to maximize the parameters accuracy and the results are

compared with standard identification profiles, such as CC and multistep discharging approaches. A sub-optimal approach is proposed in order to reduce the computational burden, which may be a limiting factor in the design of experiments of long time duration, which plays a key role in parameters identification accuracy. The results show that the proposed methodology outperforms standard approaches in terms of time required for the convergence of the parameters when the SPMe is assumed to be the real plant. Subsequently, the P2D model is considered as the real plant and the SPMe used as model for the control. Also in this case, the optimal experimental design for identifying the parameters of the SPMe provides the best results during validation. Future works may include experimental validation of the proposed strategy.

8 Supporting information

In the Supporting Information file we include the tables with the parameters of the P2D model used in the simulations, in order to increase their reproducibility.

References

- (1) Chaturvedi, N. A.; Klein, R.; Christensen, J.; Ahmed, J.; Kojic, A. Algorithms for advanced battery-management systems. *IEEE Contr. Syst. Mag.* **2010**, *30*, 49–68.
- (2) Doyle, M.; Fuller, T. F.; Newman, J. Modeling of galvanostatic charge and discharge of the lithium/polymer/insertion cell. *J. Electrochem. Soc.* **1993**, *140*, 1526–1533.
- (3) Doyle, M.; Marc, C. Design and simulation of lithium rechargeable batteries. Ph.D. thesis, 1995.
- (4) Torchio, M.; Magni, L.; Gopaluni, R. B.; Braatz, R. D.; Raimondo, D. M. LIONSIMBA:

- A Matlab Framework Based on a Finite Volume Model Suitable for Li-Ion Battery Design, Simulation, and Control. *J. Electrochem. Soc.* **2016**, *163*, A1192–A1205.
- (5) Kovatchev, B. P.; Breton, M.; Dalla Man, C.; Cobelli, C. In silico preclinical trials: a proof of concept in closed-loop control of type 1 diabetes. 2009.
- (6) Ecker, M.; Tran, T. K. D.; Dechent, P.; Käbitz, S.; Warnecke, A.; Sauer, D. U. Parameterization of a physico-chemical model of a lithium-ion battery I. Determination of parameters. *J. Electrochem. Soc.* **2015**, *162*, A1836–A1848.
- (7) Bizeray, A. State and parameter estimation of physics-based lithium-ion battery models. Ph.D. thesis, University of Oxford, 2016.
- (8) Lopez, C. D.; Wozny, G.; Flores-Tlacuahuac, A.; Vasquez-Medrano, R.; Zavala, V. M. A Computational Framework for Identifiability and Ill-Conditioning Analysis of Lithium-Ion Battery Models. *Ind. Eng. Chem. Res.* **2016**, *55*, 3026–3042.
- (9) Akaike, H. *Selected Papers of Hirotugu Akaike*; Springer, 1998; pp 199–213.
- (10) Forman, J. C.; Moura, S. J.; Stein, J. L.; Fathy, H. K. Genetic identification and fisher identifiability analysis of the Doyle–Fuller–Newman model from experimental cycling of a LiFePO₄ cell. *J. Power Sources* **2012**, *210*, 263–275.
- (11) Zhang, L.; Lyu, C.; Hinds, G.; Wang, L.; Luo, W.; Zheng, J.; Ma, K. Parameter sensitivity analysis of cylindrical lifepo₄ battery performance using multi-physics modeling. *J. Electrochem. Soc.* **2014**, *161*, A762–A776.
- (12) Moura, S. J. Estimation and control of battery electrochemistry models: A tutorial. Decision and Control (CDC), 2015 IEEE 54th Annual Conference on. 2015; pp 3906–3912.
- (13) Lu, L.; Han, X.; Li, J.; Hua, J.; Ouyang, M. A review on the key issues for lithium-ion battery management in electric vehicles. *J. Power Sources* **2013**, *226*, 272–288.

- (14) He, H.; Xiong, R.; Fan, J. Evaluation of lithium-ion battery equivalent circuit models for state of charge estimation by an experimental approach. *Energies* **2011**, *4*, 582–598.
- (15) Tian, N.; Wang, Y.; Chen, J.; Fang, H. On parameter identification of an equivalent circuit model for lithium-ion batteries. Control Technology and Applications (CCTA), 2017 IEEE Conference on. 2017; pp 187–192.
- (16) Torchio, M.; Wolff, N. A.; Raimondo, D. M.; Magni, L.; Krewer, U.; Gopaluni, R. B.; Paulson, J. A.; Braatz, R. D. Real-time model predictive control for the optimal charging of a lithium-ion battery. American Control Conference (ACC), 2015. 2015; pp 4536–4541.
- (17) Torchio, M.; Magni, L.; Braatz, R. D.; Raimondo, D. Design of Piecewise Affine and Linear Time-Varying Model Predictive Control Strategies for Advanced Battery Management Systems. *J. Electrochem. Soc.* **2017**, *164*, A949–A959.
- (18) Santhanagopalan, S.; Guo, Q.; Ramadass, P.; White, R. E. Review of models for predicting the cycling performance of lithium ion batteries. *J. Power Sources* **2006**, *156*, 620–628.
- (19) Di Domenico, D.; Stefanopoulou, A.; Fiengo, G. Lithium-ion battery state of charge and critical surface charge estimation using an electrochemical model-based extended Kalman filter. *J. Dyn. Syst., Meas., Control* **2010**, *132*, 061302.
- (20) Bizeray, A. M.; Kim, J.-H.; Duncan, S. R.; Howey, D. A. Identifiability and parameter estimation of the single particle lithium-ion battery model. *IEEE T. Contr. Syst. T.* **2018**, 1–16.
- (21) Schmidt, A. P.; Bitzer, M.; Imre, Á. W.; Guzzella, L. Experiment-driven electrochemical modeling and systematic parameterization for a lithium-ion battery cell. *J. Power Sources* **2010**, *195*, 5071–5080.

- (22) Moura, S. J.; Argomedeo, F. B.; Klein, R.; Mirtabatabaei, A.; Krstic, M. Battery state estimation for a single particle model with electrolyte dynamics. *IEEE T. Contr. Syst. T.* **2017**, *25*, 453–468.
- (23) Pukelsheim, F. *Optimal design of experiments*; Siam, 1993; Vol. 50.
- (24) Liu, J.; Rothenberger, M.; Mendoza, S.; Mishra, P.; Jung, Y.-s.; Fathy, H. K. Can an identifiability-optimizing test protocol improve the robustness of subsequent health-conscious lithium-ion battery control? an illustrative case study. American Control Conference (ACC), 2016. 2016; pp 6320–6325.
- (25) Mendoza, S.; Rothenberger, M.; Hake, A.; Fathy, H. Optimization and experimental validation of a thermal cycle that maximizes entropy coefficient fisher identifiability for lithium iron phosphate cells. *J. Power Sources* **2016**, *308*, 18–28.
- (26) Mendoza, S.; Rothenberger, M.; Liu, J.; Fathy, H. K. Maximizing Parameter Identifiability of a Combined Thermal and Electrochemical Battery Model Via Periodic Current Input Optimization. *IFAC PapersOnLine* **2017**, *50*, 7314–7320.
- (27) Hametner, C.; Jakubek, S. State of charge estimation for lithium ion cells: Design of experiments, nonlinear identification and fuzzy observer design. *J. Power Sources* **2013**, *238*, 413–421.
- (28) Mathieu, R.; Baghdadi, I.; Briat, O.; Gyan, P.; Vinassa, J.-M. D-optimal design of experiments applied to lithium battery for ageing model calibration. *Energy* **2017**, *141*, 2108–2119.
- (29) Park, S.; Kato, D.; Gima, Z.; Klein, R.; Moura, S. Optimal Experimental Design for Parameterization of an Electrochemical Lithium-Ion Battery Model. *J. Electrochem. Soc.* **2018**, *165*, A1309–A1323.

- (30) Körkel, S.; Kostina, E. *Modeling, simulation and optimization of complex processes*; Springer, 2005; pp 255–272.
- (31) Ramadass, P.; Haran, B.; Gomadam, P. M.; White, R.; Popov, B. N. Development of First Principles Capacity Fade Model for Li-Ion Cells. *J. Electrochem. Soc.* **2004**, *151*, A196.
- (32) Northrop, P. W.; Ramadesigan, V.; De, S.; Subramanian, V. R. Coordinate transformation, orthogonal collocation, model reformulation and simulation of electrochemical-thermal behavior of lithium-ion battery stacks. *J. Electrochem. Soc.* **2011**, *158*, A1461–A1477.
- (33) Moura, S. J.; Chaturvedi, N. A.; Krstic, M. PDE estimation techniques for advanced battery management systems Part I: SOC estimation. American Control Conference (ACC), 2012. 2012; pp 559–565.
- (34) Tanim, T. R.; Rahn, C. D.; Wang, C. State of charge estimation of a lithium ion cell based on a temperature dependent and electrolyte enhanced single particle model. *Energy* **2015**, *80*, 731–739.
- (35) Chaturvedi, N. A.; Klein, R.; Christensen, J.; Ahmed, J.; Kojic, A. Modeling, estimation, and control challenges for lithium-ion batteries. American Control Conference (ACC), 2010. 2010; pp 1997–2002.
- (36) Bizeray, A. M.; Zhao, S.; Duncan, S. R.; Howey, D. A. Lithium-ion battery thermal-electrochemical model-based state estimation using orthogonal collocation and a modified extended Kalman filter. *J. Power Sources* **2015**, *296*, 400–412.
- (37) Subramanian, V. R.; Diwakar, V. D.; Tapriyal, D. Efficient macro-micro scale coupled modeling of batteries. *J. Electrochem. Soc.* **2005**, *152*, A2002–A2008.
- (38) Bellman, R.; Åström, K. J. On structural identifiability. *Math. Biosci.* **1970**, *7*, 329–339.

- (39) Cobelli, C.; Distefano 3rd, J. J. Parameter and structural identifiability concepts and ambiguities: a critical review and analysis. *Am. J. Physiol.-Reg. I.* **1980**, *239*, R7–R24.
- (40) Andersson, J.; Åkesson, J.; Diehl, M. CasADi – A symbolic package for automatic differentiation and optimal control. *Recent Advances in Algorithmic Differentiation*. Berlin, 2012; pp 297–307.
- (41) Belsley, D. A.; Kuh, E.; Welsch, R. E. *Regression diagnostics: Identifying influential data and sources of collinearity*; John Wiley & Sons, 2005; Vol. 571.
- (42) Lopez, C. D.; Barz, T.; Körkel, S.; Wozny, G. Nonlinear ill-posed problem analysis in model-based parameter estimation and experimental design. *Comput. Chem. Eng.* **2015**, *77*, 24–42.
- (43) Golub, G. H.; Reinsch, C. Singular value decomposition and least squares solutions. *Numer. Math.* **1970**, *14*, 403–420.
- (44) Cover, T. M.; Thomas, J. A. *Elements of information theory*; John Wiley & Sons, 2012.
- (45) Körkel, S.; Kostina, E.; Bock, H. G.; Schlöder, J. P. Numerical methods for optimal control problems in design of robust optimal experiments for nonlinear dynamic processes. *Optim. Method. Softw.* **2004**, *19*, 327–338.
- (46) Nocedal, J.; Wright, S. J. *Nonlinear Equations*; Springer, 2006.
- (47) Potra, F. A.; Wright, S. J. Interior-point methods. *J. Comput. Appl. Math.* **2000**, *124*, 281–302.
- (48) Wächter, A.; Biegler, L. T. On the implementation of an interior-point filter line-search algorithm for large-scale nonlinear programming. *Math. Program.* **2006**, *106*, 25–57.

Graphical TOC Entry

